Nonequilibrium spin transport on Au(111) surfaces

Ming-Hao Liu,[1,*] Son-Hsien Chen,[1,2] and Ching-Ray Chang[1]

[1] *Department of Physics, National Taiwan University, Taipei 10617, Taiwan*
[2] *Department of Physics and Astronomy, University of Delaware, Newark, DE 19716-2570, USA*

(Dated: October 18, 2008)

The well-known experimentally observed *sp*-derived Au(111) Shockley surface states with Rashba spin splitting are perfectly fit by an effective tight-binding model, considering a two-dimensional hexagonal lattice with p_z-orbital and nearest neighbor hopping only. The extracted realistic band parameters are then imported to perform the Landauer-Keldysh formalism to calculate nonequilibrium spin transport in a two-terminal setup sandwiching a Au(111) surface channel. Obtained results show strong spin density on the Au(111) surface and demonstrate (i) intrinsic spin-Hall effect, (ii) current-induced spin polarization, and (iii) Rashba spin precession, all of which have been experimentally observed in semiconductor heterostructures, but not in metallic surface states. We therefore urge experiments in the latter for these spin phenomena.

PACS numbers: 73.20.At, 73.23.-b, 71.70.Ej

I. INTRODUCTION

Two-dimensional electron gas (2DEG) is known to exist in various systems, including semiconductor heterostructures[1] and metallic surface states.[2] Due to the lack of inversion symmetry introduced by the interface or surface, the spin degeneracy, the combining consequence of the time reversal symmetry (Kramers degeneracy) and the inversion symmetry, is removed and the energy dispersion becomes spin-split. In semiconductor heterostructures, one of the underlying mechanisms leading to such spin splitting is known as the Rashba spin-orbit coupling,[3] which stimulates a series of discussion on plenty of intriguing spin-dependent phenomena. Well studied phenomena include spin precession,[4,5] spin-Hall effect (SHE),[6,7,8] and current-induced spin polarization (CISP),[7,8,9,10] all of which have been experimentally observed in semiconductor heterostructures. Contrarily, none of these in metallic surface states is reported, even though the Rashba effect has been shown to exist therein.[11,12]

To the lowest order in the inplane wave vector $k_\parallel$, the two spin-split energy branches are expressed as $E_\pm = \hbar^2 k_\parallel^2/2m^\star \pm \alpha k_\parallel$ ($m^\star$ the electron effective mass), so that the Rashba spin splitting $\Delta E = E_+ - E_- = 2\alpha k_\parallel$ is linear in $k_\parallel$. Here the proportional constant α is commonly referred to as the Rashba coupling constant or the Rashba parameter. Typical values of α in semiconductor heterostructures are at most of the order of 10^{-2} eV Å,[7,10,13] while in metallic surface states α can be one or two orders larger.

The first evidence of spin splitting in metallic surface states was pioneered by LaShell *et al.* on Au(111) surfaces at room temperature.[11] The origin of their observed spin splitting was later recognized as the Rashba effect by performing the first-principles electronic-structure and photoemission calculations,[14,15] which are in good agreement with the spin-resolved photoemission experiments.[15,16] Concluded Rashba parameter of the Au(111) surface states is about $\alpha = 0.36$ eV Å. Subsequent findings of giant Rashba spin-orbit coupling is also claimed in Bi(111) surfaces[17] with $\alpha \approx 0.83$ eV Å and in Bi/Ag(111) surface alloy[18] with $\alpha \approx 3.05$ eV Å.

It is therefore legitimate to expect the previously mentioned spin-dependent phenomena to be observed on those metallic surfaces with strong Rashba coupling. In this paper we theoretically study nonequilibrium spin transport in 2DEG held by Au(111) surface states, which exhibit not only strong Rashba coupling but also simple parabola-like dispersions.[19] The latter characteristic enables successful description of the band structure using the simplest tight-binding model (TBM), which then provides the Landauer-Keldysh formalism (LKF)[20,21,22] with reasonable or even realistic band parameters.

This paper is organized as follows. In Sec. II we de-

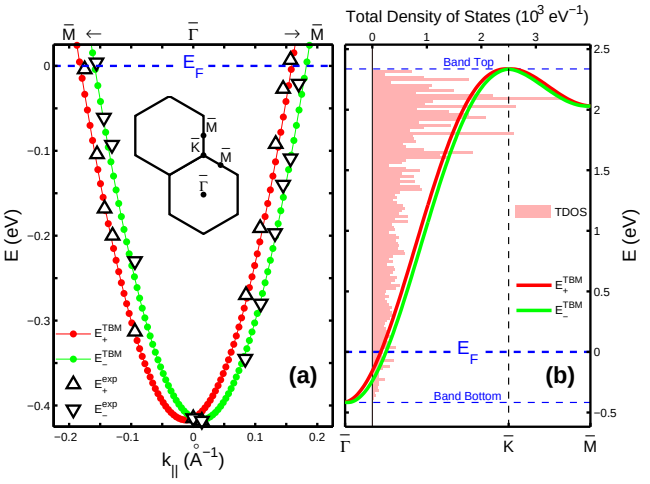

FIG. 1: (Color online) (a) Tight-binding energy dispersion $E_\pm^{\rm TBM}$ and the experimentally measured binding energy $E_\pm^{\rm exp}$ of Ref. 11, along the $\bar\Gamma\bar M$ direction. The surface Brillouin zone is sketched in the inset. (b) Total density of states and $E_\pm^{\rm TBM}$ along $\bar\Gamma\bar K$ and $\bar K\bar M$ directions.

scribe the Au(111) surface band structure by using an effective TBM, through which the experimentally measured energy dispersions[11] can be perfectly reproduced. Section III is devoted to nonequilibrium spin transport on a finite Au(111) surface channel attached to two external leads, using the LKF with band parameters extracted in Sec. II. The intrinsic SHE, the CISP, and the Rashba spin precession will be shown by directly imaging the local spin densities. We conclude in Sec. IV.

II. Au(111) SURFACE BAND STRUCTURE

A. Effective tight-binding model

We first demonstrate that the *sp*-derived Shockley surface states on Au(111) from Ref. 11 can be well described by an effective TBM [see Fig. 1(a)] for a single sheet of two-dimensional hexagonal lattice, taking into account only p_z-orbital hopping between nearest neighbors, subject to the Rashba spin-orbit coupling. The Hamiltonian matrix can be written as[23,24]

$$\mathbb{H} = E_p \mathbb{1} + \sum_{\mathbf{t}_I} e^{i\mathbf{k}_\parallel \cdot \mathbf{t}_I} \left[V_{pp\pi} \mathbb{1} + V_R \mathbf{e}_z \cdot (\vec{\sigma} \times \mathbf{t}_I) \right], \quad (1)$$

where $\mathbb{1}$ is the 2×2 identity matrix, E_p is the p-orbital energy, $\mathbf{t}_I$ represents the six nearest neighbor hopping vectors, $V_{pp\pi}$ is the band parameter describing the orbital integral under the two-center approximation of Slater and Koster,[25] V_R is the Rashba hopping parameter, and $\vec{\sigma} = (\sigma_x, \sigma_y, \sigma_z)$ is the Pauli matrix vector. The three terms in Eq. (1) are the energy band offset, the kinetic hopping, and the Rashba hopping, respectively. Arranging the two primitive translation vectors for the hexagonal lattice as $\mathbf{t}_1 = (\sqrt{3}/2, 1/2, 0)a$ and $\mathbf{t}_2 = (-\sqrt{3}/2, 1/2, 0)a$ where a is the lattice constant, the six nearest neighbor hopping vectors are $\mathbf{t}_I = \pm\mathbf{t}_1, \pm\mathbf{t}_2, \pm(\mathbf{t}_1 + \mathbf{t}_2)$, and Eq. (1) then takes the explicit form of

$$\mathbb{H}(\mathbf{k}_\parallel) = \begin{pmatrix} E_p + G(\mathbf{k}_\parallel) & F(\mathbf{k}_\parallel) \\ F^*(\mathbf{k}_\parallel) & E_p + G(\mathbf{k}_\parallel) \end{pmatrix} \quad (2)$$

with

$$F(\mathbf{k}_\parallel) = iV_R[(1+\sqrt{3}i)\sin\mathbf{k}_\parallel \cdot \mathbf{t}_1 + (1-\sqrt{3}i)\sin\mathbf{k}_\parallel \cdot \mathbf{t}_2 + 2\sin k_y a] \quad (3)$$

$$G(\mathbf{k}_\parallel) = 2V_{pp\pi}[2\cos\frac{\sqrt{3}k_x a}{2}\cos\frac{k_y a}{2} + \cos(k_y a)]. \quad (4)$$

Equation (2) can be diagonalized to yield the energy dispersions

$$E(\mathbf{k}_\parallel) = E_p + G(\mathbf{k}_\parallel) \pm |F(\mathbf{k}_\parallel)|. \quad (5)$$

Noting from Eq. (3) that V_R is embedded in $F(\mathbf{k}_\parallel)$, the above dispersion contains the Rashba term to all (odd) orders in $k_\parallel$.

In the vicinity of $\bar{\Gamma}$, i.e., $|\mathbf{k}_\parallel|a \ll 1$, Eqs. (3) and (4) are approximated by $F(\mathbf{k}_\parallel) \approx -3V_R(k_x - ik_y)a$ and $G(\mathbf{k}_\parallel) \approx 6V_{pp\pi} - (3V_{pp\pi}a^2/2)k_\parallel^2$, respectively, and the Hamiltonian matrix (2) then takes the form

$$\mathbb{H}_{k_\parallel a \ll 1} = \begin{pmatrix} E_0 - \frac{3V_{pp\pi}a^2}{2}k_\parallel^2 & -3V_R(k_x - ik_y)a \\ -3V_R(k_x + ik_y)a & E_0 - \frac{3V_{pp\pi}a^2}{2}k_\parallel^2 \end{pmatrix}, \quad (6)$$

where $E_0 \equiv E_p + 6V_{pp\pi}$. Equation (6) is consistent with the p_z-resolved effective Hamiltonian of the earlier TBM by Petersen and Hedegård, who considered all the three p-orbitals, subject to the intra-atomic spin-orbit coupling.[26]

B. Extraction of band parameters

We now fit our tight-binding dispersions (5) with the experiment of Ref. 11. This can be done by comparing the low-$k_\parallel$ expansion of Eq. (5),

$$E(\mathbf{k}_\parallel)\big|_{ka\ll 1} \approx E_p + 6V_{pp\pi} - \frac{3V_{pp\pi}a^2}{2}k_\parallel^2 \pm 3V_R a|\mathbf{k}_\parallel|, \quad (7)$$

with that of the free-electron model, $E(k_\parallel) = E_0 + (\hbar^2/2m^\star)k_\parallel^2 \pm \alpha k_\parallel$. In addition to the band offset $E_0 = E_p + 6V_{pp\pi}$, we identity $V_{pp\pi} = -(2/3a^2)(\hbar^2/2m^\star)$ and $V_R = \alpha/3a$. Using the reciprocal vector $\mathbf{g}_1 = (4\pi/\sqrt{3}a)(1/2, \sqrt{3}/2, 0)$ and $\bar{M} = 1.26$ Å^{-1} from Ref. 11, we have $\hbar^2/2m^\star \approx 15.2$ eV Å^2, $\alpha \approx 0.3557$ eV Å, and $E_0 \approx -0.415$ eV. The norm of $\mathbf{g}_1$ gives $\bar{M}$ such that the lattice constant is $a = 4\pi/\sqrt{3}|\mathbf{g}_1| = 5.7581$ Å. Hence we deduce $V_{pp\pi} = -0.3056$ eV, $V_R = 0.0206$ eV, and $E_p = 1.4188$ eV. Substituting these parameters into Eqs. (3)–(5), a nearly perfect consistency between our effective TBM and the experimentally measured binding energy of Ref. 11 can be seen in Fig. 1(a). The experimentally measured Fermi surface of the concentric rings slightly distorted from circles[19] can be reproduced as well, but we do not explicitly show.

III. NONEQUILIBRIUM SPIN TRANSPORT

A. Landauer-Keldysh formalism vs tight-binding model

Next we apply the Landauer-Keldysh formalism,[21] namely the nonequilibrium Keldysh Green's function formalism[27] applied on Landauer multiterminal ballistic nanostructures. For detailed introduction to the LKF, see Refs. 20,22. To make use of the previously extracted band parameters in the LKF calculation, we consider the second-quantized single particle Hamiltonian,[24]

$$\mathcal{H} = \sum_n \varepsilon_n c_n^\dagger c_n + \sum_{\langle m,n \rangle} c_m^\dagger \left[t_0 + it_R (\vec{\sigma} \times \mathbf{d}_{mn})_z \right] c_n, \quad (8)$$

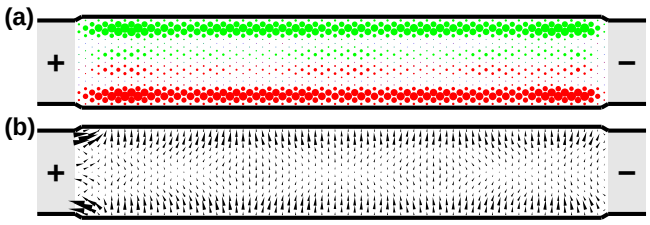

FIG. 2: (Color online) Local spin density of (a) the out-of-plane component $\langle S_z\rangle$ and (b) the inplane component ($\langle S_x\rangle, \langle S_y\rangle$) in a 398.9 ×63.3 (total number of sites $N = 931$) conducting sample made of Au(111) surface. The size of each local marker depicts the magnitude. In (a), red/dark (green/light) dots denote $\langle S_z\rangle > 0$ ($\langle S_z\rangle < 0$). The maximum of $\langle S_z\rangle$ is $1.2 \times 10^{-3}\,(\hbar/2)$ while the mean of $\langle S_y\rangle$ is $3.16 \times 10^{-4}(\hbar/2)$.

which is equivalent to Eq. (1), provided $\varepsilon_n = E_p$, $t_0 = -V_{pp\pi}$, and $t_R = V_R$. In Eq. (8), $c_n^\dagger$ (c_n) is the creation (annihilation) operator of the electron on site n, $\langle m, n\rangle$ means that sites m and n are nearest neighbors to each other, and $\mathbf{d}_{mn}$ is the unit vector pointing from n to m. Despite the different system sizes TBM and LKF consider (infinite for TBM and finite for LKF) and different functions they provide (simple band calculation by TBM and nonequilibrium transport by LKF), the equivalence of the underlying Hamiltonians should contain the same physics. The explicit correspondence can be shown by comparing the band structure by the TBM with the total density of states (TDOS) by the LKF, provided that the same parameters are used.

For the LKF calculation, we consider a $80(a\sqrt{3}/2) \times 11a \approx 398.9$ Å ×63.3 Å (total number of sites $N = 931$) channel made of an ideal Au(111) surface, in perfect contact with two unbiased normal metal leads at the left and right ends of the sample. We will further image the nonequilibrium spin transport on this two-terminal setup later. As shown in Fig. 1(b), the range of the calculated nonvanishing TDOS is consistent with the TBM dispersion along the $\bar{\Gamma}\bar{K}$ direction, which corresponds to the nearest neighbor hopping direction as we considered in the underlying Hamiltonian (8).

B. Injection of unpolarized current: Intrinsic spin-Hall effect and current-induced spin polarization

Combination of the consistency between the experimental and the TBM dispersions, and that between the dispersion by the TBM and the TDOS by the LKF, indirectly demonstrates that the following imaging of local spin densities by the LKF stands on an experimental footing. As a first demonstration of the nonequilibrium spin transport, we turn on the bias of potential difference $eV_0 = 0.2$ eV between the two normal metal leads. We will denote $\pm eV_0/2$ on the leads by ± sign. With such injection of an unpolarized electron current, we expect (i) the SHE of the intrinsic type, and (ii) the CISP, which follows the Rashba eigenspin direction of the lower energy branch. Both of these can be seen respectively in Figs. 2(a) and 2(b). The former shows an antisymmetric out-of-plane spin accumulation with $\langle S_z\rangle_{\max} = 1.2 \times 10^{-3}(\hbar/2)$ at lateral edges, while the latter shows that the inplane components of spins mostly point to $+y$ axis[28] with average value $\overline{\langle S_y\rangle} = 3.16 \times 10^{-4}(\hbar/2)$. Note that the local spin densities shown here represent, by definition, the site-dependent total number of spins.[22] Dividing $\overline{\langle S_y\rangle}$ by the hexagonal unit cell area $\sqrt{3}a^2/2$, we deduce that the obtained spin (area) density due to CISP is in average 1101 μm^{-2}, which is clearly much stronger than that observed in the CISP experiment of Ref. 9, where the spin (volume) density less than 10 μm^{-3} (corresponding to a even weaker spin area density) is reported.

C. Injection of spin-polarized current: Rashba spin precession

Next we inject spin-polarized currents by replacing the left (source) lead with a ferromagnetic electrode. Previously, the self-energy due to the normal metal lead, which is assumed to be semi-infinite, in thermal equilibrium, and in perfect contact with the sample, can be obtained by solving the surface Green's function of the lead,[20] subject to Hamiltonian $\mathcal{H}_{\text{lead}} = \mathbf{p}^2/2m + V$. The momentum operator $\mathbf{p} = (p_x, p_y)$ is two-dimensional and the potential V describes a infinite potential well of a semi-infinite rectangle shape. The exact form of the lead self-energy reads

$$\Sigma^R(p_1, p_2) = -\frac{2t}{N_d+1}\sum_{n=1}^{\infty}\sin\frac{n\pi p_1}{N_d+1}\sin\frac{n\pi p_2}{N_d+1} \times \mathbb{1}\frac{e^{ik_n a}\sin(k_n a)}{k_n a} \tag{9}$$

with $k_n a = \sqrt{(E - E_n)/t}$ and $E_n = [n\pi/(N_d+1)]^2 t$. Here $p_{1(2)} = 1, 2, \cdots, N_d$ is the lateral position (implicitly in units of lattice constant a) of the edge site in the sample in contact with the lead, t is the coupling between the sample and the lead and is usually set equal to the kinetic hopping t_0 in the sample, and $(N_d+1)\,a$ is implicitly assumed to be the width of the lead.

To take into account the exchange field inside the ferromagnetic lead, we adopt the Weiss mean field approximation and add a Zeeman term $-\mu_B\vec{\sigma}\cdot\mathbf{B}_{ex}$ ($\mu_B \approx 5.8 \times 10^{-5}\,\text{eV}\,\text{T}^{-1}$ the Bohr magneton) to $\mathcal{H}_{\text{lead}}$. Typical exchange field may be as high as $|\mathbf{B}_{ex}| \approx 10^{-3}$ T (Ref. 29), leading to $|\mu_B\mathbf{B}_{ex}| \approx 5.8 \times 10^{-2}$ eV. We will take this value in the forthcoming spin precession demonstration. The explicit form of the self-energy is obtained by substituting in Eq. (9) $k_n a \to k_n^\sigma a = \sqrt{(E - E_n + \sigma\,|\mu_B\mathbf{B}_{ex}|)/t}$ and $\mathbb{1} \to \sum_{\sigma=\pm}|\mathbf{n}\sigma\rangle\langle\mathbf{n}\sigma|$,

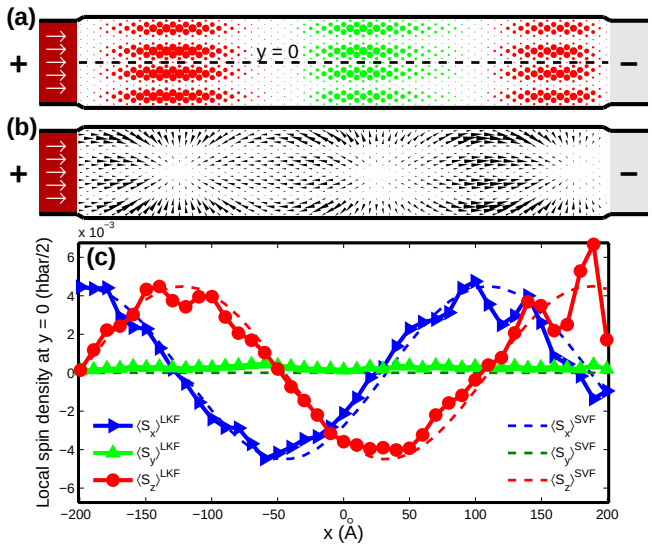

FIG. 3: (Color online) Local spin density of (a) the out-of-plane component $\langle S_z\rangle$ and (b) the inplane component $(\langle S_x\rangle, \langle S_y\rangle)$, in a conducting sample made of Au(111) surface, subject to a ferromagnetic source lead with $+x$ magnetization. (c) $\langle S_x\rangle$, $\langle S_y\rangle$, and $\langle S_z\rangle$ as a function of x at $y = 0$, i.e., along the dashed line sketched in (a). Computed values are compared with the previously obtained spin vector formula based on quantum mechanics.

where $|\mathbf{n}\sigma\rangle$ is the spin-1/2 state ket with quantization axis $\mathbf{n}$.[30]

Applying the same voltage difference of 0.2 V and magnetizing the ferromagnetic source lead along $+x$ axis, Figs. 3(a) and 3(b) show the out-of-plane and inplane components of the local spin densities, respectively. The injected x-polarized spins moving along $+x$ and encountering the Rashba effective magnetic field pointing to $-y$, are forced to precess about $-y$-axis counterclockwise, and hence the Rashba spin precession is observed. In the free electron model, the spin precession length (the distance within which the spin completes a precession angle of π) is $L_{so} = (\pi/\alpha)(\hbar^2/2m^\star) \approx 134$ Å. Thus the channel length 398.9 Å is about 3 times L_{so}, which is consistent to what we observe in Figs. 3(a) and 3(b). Note that here the SHE competing with the spin precession is relatively weak due to the strong exchange field we consider in the source lead. However one can still observe the tiny asymmetry of the $\langle S_z\rangle$ pattern of Fig. 3(a) along the lateral direction (more $+\langle S_z\rangle$ and $-\langle S_z\rangle$ accumulations near the bottom and top edges, respectively). In the following we will concentrate on the spin precession only.

To compare the LKF results with the free electron model in further detail, we recall the spin vector formula [see Eq. (6) of Ref. 31], which takes the form of $(\langle S_x\rangle, \langle S_y\rangle, \langle S_z\rangle) = (\cos\Delta\theta, 0, \sin\Delta\theta)$ here with $\Delta\theta = (2m^\star/\hbar^2)\alpha x = 2.34\times10^{-2}x$, where x is in unit of Å. Note that a factor of $\sqrt{3}/2$ responsible for the net and actual hopping distances has to be taken into account in x, since the crystal structure information remains. Accordingly, good agreement between the LKF and the spin vector formula can be seen in Fig. 3(c). Note that in view of both Figs. 2 and 3, size and edge effects, arising from the charge distribution, are also observed. The former, the size effect, appears in the modulation along y direction with roughly 4 peaks corresponding to a wave length≈ 32 Å, roughly shorter than the Fermi wavelength $2\pi/k_F \approx 38$ Å; the latter, the edge effect, appears in the abnormal charge accumulation near the side and drain edges.

IV. CONCLUSION

In conclusion, we have shown that the *sp*-derived Shockley surface states on Au(111),[11,14,15,16,19] which extend over the first few layers though, can be well described by an effective TBM for a two-dimensional hexagonal lattice, taking into account p_z-orbital and nearest neighbor hopping only. Required parameters in the nonequilibrium spin transport calculation by the LKF, demonstrating (i) intrinsic SHE and CISP due to injection of unpolarized current and (ii) the Rashba spin precession due to injection of spin-polarized current, thus stand on an experimental footing of the pioneering work of LaShell *et. al.*.[11] Calculated local spin densities in all the three spin phenomena are much stronger than those in semiconductor heterostructures. Whereas the magnetic optical Kerr effect (MOKE) can sensitively detect a spin volume density of less than 10 spins per μm^3 (Ref. 9), our results of more than 10^3 spins per μm^2 suggest definitely measurable nonequilibrium spin transport supported by the Au(111) surface states and others with even stronger Rashba coupling such as Bi(111) surfaces[17] or Bi/Ag(111) surface alloys.[18] Last, in addition to the stronger local spin densities induced by stronger Rashba coupling, the spin precession length (typically of the order of 1 μm in semiconductor heterostructures) in these surface states is greatly reduced [134 Å for Au(111) reported here], such that the fine structure of the spin patterns due to spin precession or the intrinsic SHE requires high resolution apparatus such as the spin-polarized scanning tunneling microscopy.[32]

Acknowledgments

Financial support of the Republic of China National Science Council Grant No. 95-2112-M-002-044-MY3 is gratefully acknowledged.

* Present address: No. 2-1, Fushou Lane, Chengsiang Village, Gangshan Township, Kaohsiung County 82064, Taiwan; Electronic address: d92222010@ntu.edu.tw

[1] J. H. Davies, *The Physics of Low-Dimensional Semiconductors* (Cambridge University Press, Cambridge, U.K., 1998).

[2] S. G. Davison and M. Stęślicka, *Basic Theory of Surface States* (Oxford University Press, Oxford, U.K., 1992).

[3] Y. A. Bychkov and E. I. Rashba, JETP Lett. **39**, 78 (1984).

[4] Y. Kato, R. C. Myers, A. C. Gossard, and D. D. Awschalom, Nature **427**, 50 (2004).

[5] S. A. Crooker and D. L. Smith, Phys. Rev. Lett. **94**, 236601 (2005).

[6] Y. K. Kato, R. C. Myers, A. C. Gossard, and D. D. Awschalom, Science **306**, 1910 (2004).

[7] V. Shi, R. C. Myers, Y. K. Kato, W. H. Lau, A. C. Gossard, and D. D. Awschalom, Nat. Phys. **1**, 31 (2005).

[8] N. P. Stern, S. Ghosh, G. Xiang, M. Zhu, N. Samarth, and D. D. Awschalom, Phys. Rev. Lett. **97**, 126603 (2006).

[9] Y. K. Kato, R. C. Myers, A. C. Gossard, and D. D. Awschalom, Phys. Rev. Lett. **93**, 176601 (2004).

[10] C. L. Yang, H. T. He, L. Ding, L. J. Cui, Y. P. Zeng, J. N. Wang, and W. K. Ge, Phys. Rev. Lett. **96**, 186605 (2006).

[11] S. LaShell, B. A. McDougall, and E. Jensen, Phys. Rev. Lett. **77**, 3419 (1996).

[12] G. Bihlmayer, Y. M. Koroteev, P. M. Echenique, E. V. Chulkov, and S. Blügel, Surf. Sci. **600**, 3888 (2006).

[13] J. Nitta, T. Akazaki, H. Takayanagi, and T. Enoki, Phys. Rev. Lett. **78**, 1335 (1997).

[14] J. Henk, A. Ernst, and P. Bruno, Phys. Rev. B **68**, 165416 (2003).

[15] J. Henk, M. Hoesch, J. Osterwalder, A. Ernst, and P. Bruno, J. Phys.: Condens. Matter **16**, 7581 (2004).

[16] M. Hoesch, M. Muntwiler, V. N. Petrov, M. Hengsberger, L. Patthey, M. Shi, M. Falub, T. Greber, and J. Osterwalder, Phys. Rev. B **69**, 241401(R) (2004).

[17] Y. M. Koroteev, G. Bihlmayer, J. E. Gayone, E. V. Chulkov, S. Blügel, P. M. Echenique, and P. Hofmann, Phys. Rev. Lett. **93**, 046403 (2004).

[18] C. R. Ast, J. Henk, A. Ernst, L. Moreschini, M. C. Falub, D. Pacile, P. Bruno, K. Kern, and M. Grioni, Phys. Rev. Lett. **98**, 186807 (2007).

[19] F. Reinert, J. Phys.: Condens. Matter **15**, S693 (2003).

[20] S. Datta, *Electronic Transport in Mesoscopic Systems* (Cambridge University Press, Cambridge, 1995).

[21] B. K. Nikolic, S. Souma, L. P. Zarbo, and J. Sinova, Phys. Rev. Lett. **95**, 046601 (2005).

[22] B. K. Nikolic, L. P. Zarbo, and S. Souma, Phys. Rev. B **73**, 075303 (2006).

[23] G. Grosso and G. P. Parravicini, *Solid State Physics* (Academic Press, 2000).

[24] C. L. Kane and E. J. Mele, Phys. Rev. Lett. **95**, 146802 (2005).

[25] J. C. Slater and G. F. Koster, Phys. Rev. **94**, 1498 (1954).

[26] L. Petersen and P. Hedegård, Surf. Sci. **459**, 49 (2000).

[27] L. V. Keldysh, Sov. Phys. JETP **20**, 1018 (1965).

[28] M.-H. Liu, S.-H. Chen, and C.-R. Chang (2008), arXiv:0802.0366v2.

[29] C. Kittel, *Introduction to Solid State Physics* (Wiley, 2005), 8th ed.

[30] J. J. Sakurai, *Modern Quantum Mechanics* (Addison-Wesley, New York, 1994), revised ed.

[31] M.-H. Liu, K.-W. Chen, S.-H. Chen, and C.-R. Chang, Phys. Rev. B **74**, 235322 (2006).

[32] M. Bode, Rep. Prog. Phys. **66**, 523 (2003).